

MIT Open Access Articles

*Cascaded Cavities Boost the Indistinguishability
of Imperfect Quantum Emitters*

The MIT Faculty has made this article openly available. **Please share**
how this access benefits you. Your story matters.

Citation: Choi, Hyeongrak et al., "Cascaded Cavities Boost the Indistinguishability of Imperfect Quantum Emitters." Physical Review Letters 122, 18 (May 2019): 183602 ©2019 Authors

As Published: <https://dx.doi.org/10.1103/PHYSREVLETT.122.183602>

Publisher: American Physical Society (APS)

Persistent URL: <https://hdl.handle.net/1721.1/129687>

Version: Final published version: final published article, as it appeared in a journal, conference proceedings, or other formally published context

Terms of Use: Article is made available in accordance with the publisher's policy and may be subject to US copyright law. Please refer to the publisher's site for terms of use.



Cascaded Cavities Boost the Indistinguishability of Imperfect Quantum Emitters

Hyeonrak Choi,^{1,*} Di Zhu,¹ Yoseob Yoon,² and Dirk Englund^{1,†}

¹Research Laboratory of Electronics, Massachusetts Institute of Technology, Cambridge, Massachusetts 02139, USA

²Department of Chemistry, Massachusetts Institute of Technology, Cambridge, Massachusetts 02139, USA



(Received 3 December 2018; published 10 May 2019)

Recently, Grange *et al.* [Phys. Rev. Lett. **114**, 193601 (2015)] showed the possibility of single-photon generation with a high indistinguishability from a quantum emitter despite strong pure dephasing, by “funneling” emission into a photonic cavity. Here, we show that a cascaded two-cavity system can further improve the photon characteristics and greatly reduce the Q factor requirement to levels achievable with present-day technology. Our approach leverages recent advances in nanocavities with an ultrasmall mode volume and does not require ultrafast excitation of the emitter. These results were obtained by numerical and closed-form analytical models with strong emitter dephasing, representing room-temperature quantum emitters.

DOI: 10.1103/PhysRevLett.122.183602

Sources of indistinguishable single photons play an essential role in quantum information science [1], including linear-optics quantum computing [2–4], precision measurements [5], quantum simulation [6], boson sampling [7,8], and all-optical quantum repeaters [9,10]. Single-photon sources based on atomlike quantum emitters have seen remarkable progress [11–15], including, in particular, color centers in diamond, many of which have been shown to possess long spin coherence times. However, a remaining challenge is to improve their emission properties to achieve near-unity indistinguishability and high collection efficiency [14,15].

Here, we show that the emission can be tailored by coupling an emitter to a cascaded two-cavity system, which provides enough control to minimize the detrimental effects of pure dephasing and spectral diffusion. Our analysis shows that the cascaded cavity improves on the photon emission efficiency (η) and indistinguishability (I) compared to previously considered single-cavity approaches. For the especially difficult problem of room-temperature operation with silicon vacancy centers in diamond, the cascaded-cavity system enables the same efficiency, but a much higher indistinguishability (~ 0.95) than, the single-cavity case (~ 0.80), with $\times 20$ lower cavity quality factor (Q factor). When the cavities are tuned for a maximum ηI product, more than 2 orders of magnitude improvement compared to the bare emitter and an $\sim 17\%$ improvement over the best single-cavity system are possible.

As shown in Fig. 1(a), the linewidth of an emitter is given by $\Gamma = \gamma + \gamma^* + \Delta\delta \gg \gamma$ at room temperature, where γ is the radiative decay rate, γ^* the pure dephasing rate, and $\Delta\delta$ the FWHM width of the spectral diffusion. Pure dephasing can be modeled as a Markovian phase flip process that occurs much faster than the excited-state lifetime. On the other hand, $\Delta\delta$ captures the spectral wandering between

photoemission events (for example, due to changing stray electric fields near the emitter) that changes much slower than the excited-state lifetime; thus, spectral diffusion can be treated by a statistical average over the ensemble. The indistinguishability, which is approximately given by

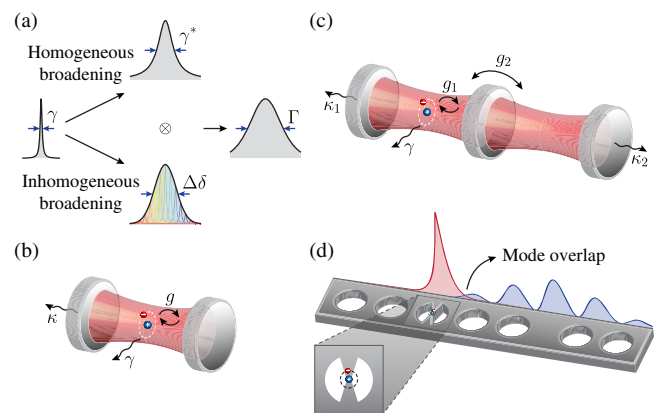


FIG. 1. (a) The emission spectrum with width Γ can be considered as a convolution of different broadenings: natural broadening (Lorentzian linewidth γ), pure dephasing (Lorentzian linewidth γ^*), and spectral diffusion (Gaussian linewidth $\Delta\delta$). (b) Cavity-QED system, where g is the coupling rate, κ is the cavity decay rate, and γ is the spontaneous emission rate of the emitter to noncavity modes. (c) Cascaded-cavity system as a room-temperature single-photon source. An emitter is coupled to the first cavity (C_1) with coupling strength g_1 . C_1 is coupled to the second cavity (C_2) with coupling strength g_2 . κ_1 and κ_2 are the cavity radiation losses to free space. (d) Photonic crystal realization of the proposed cascaded-cavity-emitter system. The first cavity produces a high emitter-cavity coupling (g_1) due to the field concentration in concentric dielectric tips; see [16,17]. A mode overlap of cavities corresponds to a cavity-cavity coupling rate of g_2 .

$I \sim \gamma/\Gamma$ [18], is vanishingly small at room temperature ($\sim 10^{-4}$ for silicon vacancy centers in nanodiamond [19]).

Nanophotonic structures have been investigated to improve I by modifying the local density of electromagnetic states (LDOS) [20]. This approach can be analyzed in its simplest form in the cavity quantum electrodynamics (cavity-QED) picture in Fig. 1(b), where $g \propto 1/\sqrt{V_{\text{eff}}}$ is the emitter-cavity coupling rate, V_{eff} the cavity mode volume, $\kappa \propto 1/Q$ the cavity decay rate, and Q the quality factor. For simplicity, we first ignore spectral diffusion, i.e., $\Gamma = \gamma + \gamma^*$. In the incoherent regime, where $\Gamma + \kappa \gg 2g$, the system dynamics reduces to a set of rate equations, in which the emitter and the cavity field pump each other at the rate $R = 4g^2/(\Gamma + \kappa)$ [21].

There are two main approaches to increase I . One strategy is to maximize the LDOS with a plasmonic cavity, so that $R = 4g^2/(\Gamma + \kappa) > \gamma^*$ [34,35]. Peyskens, Chang, and Englund [34] showed that, for a 20 nm silver nanosphere ($Q \sim 15$) coupled to a waveguide, the indistinguishability of single photons emitted from SiV can be increased to $I \sim 0.27$ while reaching a single-photon outcoupling efficiency of $\eta \sim 0.053$. On the other hand, Wein *et al.* could theoretically achieve $I \sim 0.37$ and $\eta \sim 0.77$ with the plasmonic Fabry-Perot hybrid cavity ($Q \sim 986$) recently proposed in Ref. [36]. However, this approach also faces several important obstacles: (i) the assumption of instantaneous pumping on the femtosecond scale, which is demanding due to ionization (resonant) and slow phonon relaxation (nonresonant) [37], and (ii) Ohmic and quenching losses in the metal.

A second approach investigated by Grange *et al.* [38] relies on coupling the emitter to a dielectric cavity with ultrahigh Q , which avoids the problems of high losses in metals. When the cavity decay rate κ is much smaller than γ and R , near-unity indistinguishability becomes possible. Notably, this system outperforms the spectral filtering of an emitted photon, due to a “funneling” of emission into the narrow-band cavity spectrum. However, reaching an indistinguishability of 0.9 (0.5) for an emitter with $\gamma \sim 2\pi \times 100$ MHz radiative linewidth at $\omega \sim 2\pi \times 400$ THz requires a cavity with very high $Q \sim 4 \times 10^7$ [6]; this Q far exceeds the highest quality factor nanocavity coupled to a quantum emitter, which has $Q \sim 55000$ [39]. The underlying problem is that high indistinguishability is not possible with the limited Q and V_{eff} that are currently available.

The cascaded two-cavity system considered in this paper, illustrated in Fig. 1(c), greatly reduces the Q factor requirements while obtaining higher overall single-photon source performance. The emitter is assumed to be dipole coupled with the first cavity (C_1). This cavity can have a relatively low Q factor $< 10^5$, as long as it has a small V_{eff} to efficiently collect the emitter fluorescence. However, the indistinguishability I of the emission from cavity C_1 would be low. A high I can then be achieved by coupling to a

second cavity (C_2), which provides additional degrees of freedom to optimize the single-photon emission from the system.

To investigate the dynamics quantitatively, we assume a strong pure dephasing, $\gamma^* = 10^4$, normalized to $\gamma = 1$. In the regime where the total dephasing (Γ) exceeds the emitter- C_1 coupling rate g_1 , the population transfer rate between the emitter and C_1 becomes [21]

$$R_1 = \frac{4g_1^2}{\Gamma + \kappa_1} \frac{1}{1 + \left(\frac{2\delta}{\Gamma + \kappa_1}\right)^2}, \quad (1)$$

where δ is the detuning, assumed to be 0 for now. A large transfer rate $R_1 > \gamma$ (implying $g_1 \gg 1$) is required for efficient emission into the cavity. To this end, we make use of a new cavity design using a dielectric concentrator in a photonic crystal (PhC) nanocavity [Fig. 1(d)] [16,17]. This nanocavity enables an arbitrarily small mode volume [16]; indeed, recently $V_{\text{eff}} = 10^{-3}(\lambda/n_{\text{Si}})^3$ was experimentally demonstrated in a silicon PhC [40] with a quality factor of $\sim 10^5$. Here, we consider $g_1 = 500$ and $\kappa_1 = 50$, corresponding to $V_{\text{eff}} = 0.007(\lambda/n_{\text{diamond}})^3$ and $Q \sim 50000$ for the case of silicon vacancy centers in the diamond [21,41,42]. In addition, the emitter is assumed to be located at the narrow bridge section of this cavity design, where the phonon environment is similar with the nanodiamond [19].

The second cavity (C_2) is coupled to C_1 at a rate g_2 . This coupling can be adjusted through the spacing between the two PhC cavities, as shown in Fig. 1(d). We derived the population transfer rate between cavities C_1 and C_2 from the optical Bloch equations, by applying adiabatic elimination of the coherence between the cavities in the limit of $R_1 + \kappa_1 + \kappa_2 \gg 2g_2$ (see the derivation in Supplemental Material [21]). The population transfer rate between C_1 and C_2 then becomes

$$R_2 = \frac{4g_2^2}{R_1 + \kappa_1 + \kappa_2}, \quad (2)$$

where κ_2 is the decay rate of C_2 . Note that, if $R_1 \rightarrow 0$, R_2 reduces to the Purcell-enhanced emission rate. The R_1 term in the denominator effectively acts as additional decoherence. The reduction of the population transfer rate due to this additional decoherence was studied previously in the classical and continuous-wave (cw) limits, including for nonresonant excitation of a quantum dot [43] and for light transmission in an optomechanical system [44]. However, this decoherence directly impacts the indistinguishability. Thus, we investigate the *temporal dynamics* of the system using master equations and nonequilibrium Green's functions.

We applied the master equation approach to calculate I and η as a function of g_2 and κ_2 for our cascaded-cavity-emitter system. The results in Fig. 2 show two regimes of interest. In “reg. 1” of R_2 , $\kappa_2 < \kappa_1$, we find high I and

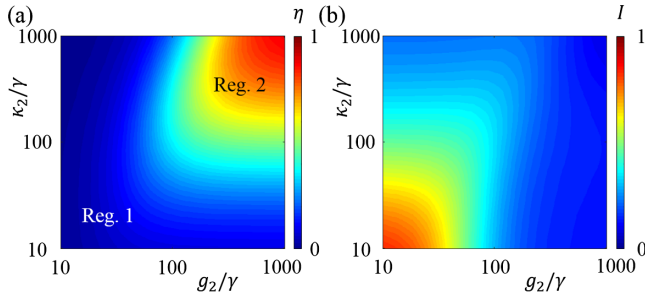


FIG. 2. Performance of the cascaded cavity system with $(g_1 = 500, \kappa_1 = 100)$ as a function of g_2 and κ_2 . Efficiency (a) and indistinguishability (b).

small η . “Reg. 2” of $R_2, \kappa_2 > \kappa_1$ leads to moderate I and large η . Analogous regimes were analyzed for a single-cavity-QED system [38]. The photon collection efficiency into C_2 follows from the Bloch equations [21] for both regimes, giving

$$\eta = \frac{\kappa_2 R_2}{\kappa_1(\kappa_2 + R_2) + \kappa_2 R_2}. \quad (3)$$

We first focus on reg. 1. When $R_1 \gg \kappa_1, \gamma$, the emitter and C_1 serves as a “composite emitter” with decoherence rate R_1 . This effective emitter decaying with a rate of $\sim \kappa_1/2$ is coupled to C_2 with $\kappa_2 < \kappa_1$ at rate $R_2/2 < \kappa_1$ (coupling is asymmetric; see Supplemental Material [21] for more details). We were able to derive an analytical form for the indistinguishability with the nonequilibrium Green’s function for the emitter-cavity system:

$$I = \frac{\kappa_1/2 + (\kappa_2 \| R_2)/2}{\kappa_1/2 + \kappa_2 + 3R_2/2}, \quad (4)$$

where $\kappa_2 \| R_2 = \kappa_2 R_2 / (\kappa_2 + R_2)$. The same result can be derived from the quantum regression theorem [35]. Note that this equation has the similar form as the one-cavity case [38] under the substitution $(\kappa_1/2, \kappa_2, R_2/2) \rightarrow (\gamma, \kappa, R)$ —i.e., we can consider the C_1 -emitter system as a composite emitter inside C_2 , and C_2 funnels the composite emitter as in Ref. [38]. Figure 3(a) plots η and I as a function of κ_2 . Equations (3) and (4) show excellent agreement with the numerical simulations with the master equations. Notice that, when $R_2 + \kappa_2 \sim R_1$, I exceeds the prediction from Eq. (4). Deviations of results from the prediction are more evident when R_1 is smaller [Fig. 3(b)]. This deviation occurs because the contribution of the coherence between cavities $[\rho_{ab}(t)]$ to the two-time correlation function of the cavity field $[\langle b^\dagger(t + \tau)b(t) \rangle]$ is not negligible [21].

Next, we investigate reg. 2 ($R_2, \kappa_2 > \kappa_1$), for which large η and moderate I are possible. In the C_1 -emitter system with $R_1 > \kappa_1$, the excitation incoherently hops back and

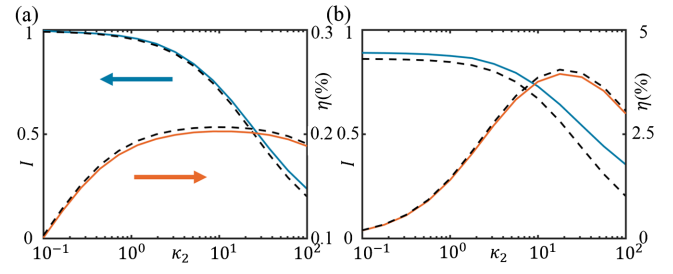


FIG. 3. High indistinguishability regime (reg. 1). The emitter and C_1 can be treated as an effective emitter coupled to C_2 with population transfer rate $R_2/2$. (a) I (blue) and η (orange) as a function of κ_2 for $(g_1, \kappa_1, g_2) = (1500, 50, 5)$. (Solid curves) Numerical result from master equation. (Dashed curves) Analytical result from Eqs. (4) (I) and (3) (η). (b) I and η vs κ_2 for $(g_1, \kappa_1, g_2) = (500, 50, 10)$. The deviation between the numerical and analytical results is due to the finite effective dephasing R_1 .

forth between the emitter and the cavity. Therefore, C_1 decoheres quickly at the rate R_1 , resulting in a low I . On the other hand, $\kappa_1 > R_1$ also results in low I , because the timing jitter of initial incoherent feeding exceeds the cavity lifetime. The solution is to choose $R_1 > \kappa_1$ and keep the population of C_1 low, preventing the photon from being reabsorbed by the emitter. C_2 provides this additional functionality with two knobs: R_2 and κ_2 . When $R_2, \kappa_2 > \kappa_1$, excitation quickly passes through C_1 , resulting in a low population of C_1 (P_{c1}). At the same time, the decoherence of the composite emitter (emitter C_1) at the rate R_1 can be suppressed by a factor of $(R_1 + \kappa_1)/(R_1 + \kappa_1 + R_2 \| \kappa_2)$.

Figure 4(a) plots I and η of the photon emitted by C_2 as a function of κ_2 , assuming $(g_1, \kappa_1, g_2) = (500, 50, 150)$. In the limit of large κ_2 and subsequently small R_2 , the dynamics of the emitter and C_1 are the same without C_2 ; C_2 merely samples the photons from C_1 . Thus, photons

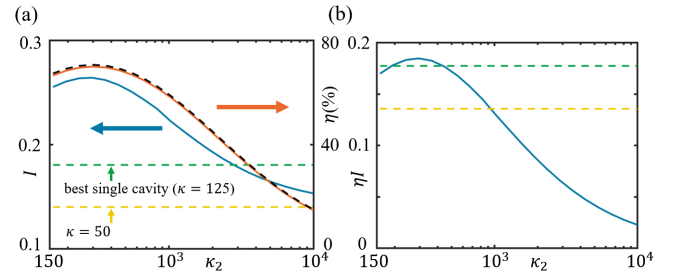


FIG. 4. Large ηI -product regime with $(g_1, \kappa_1, g_2) = (500, 50, 150)$. (a) I (blue) and η (orange) as a function of κ_2 . The black dashed line is the analytical result from Eq. (3). For a single-cavity system, I is plotted with yellow dashed ($g = 500, \kappa = 50$) and green dashed ($g = 500, \kappa = 125$) lines. The latter gives the maximum ηI of single-cavity systems. (b) ηI product as a function of κ_2 (blue line). Cascaded-cavity architecture shows higher ηI than that of a single-cavity system with $\kappa = 50$ (yellow dashed line) and $\kappa = 125$ (green dashed line, maximum ηI).

TABLE I. Comparison of the two systems.

	Cascaded cavity I , η (%), Q_1 , Q_2	Single cavity I , η (%), Q
Reg. 1	0.950, 0.76, 7000, 500 000 ^a 0.805, 3.09, 3600, 50 000 ^c	0.950, 0.25, 50 000 000 ^b 0.800, 0.27, 10 000 000 ^d
Reg. 2	0.315, 98.6, 500 000, 2100 ^e	0.267, 99.5, 3750 ^f

^a $g_1 = 500$, $\kappa_1 = 360$, $g_2 = 30$, $\kappa_2 = 5$.

^b $g = 1.33$, $\kappa = 0.05$.

^c $g_1 = 500$, $\kappa_1 = 700$, $g_2 = 87.5$, $\kappa_2 = 50$.

^d $g = 1.33$, $\kappa = 0.25$.

^e $g_1 = 500$, $\kappa_1 = 5$, $g_2 = 530$, $\kappa_2 = 1200$.

^f $g = 500$, $\kappa = 667$.

of C_2 have the same I as that of C_1 without C_2 (i.e., the single-cavity system). Simulations of the single-cavity system show that photons emitted by C_1 have $I \sim 0.14$ (shown as a yellow dashed line). Decreasing κ_2 (increasing R_2) suppresses the population of C_1 , increasing I . Since C_2 suffers from the same incoherent hopping and jitter effects as C_1 discussed above, I is maximized to $I = 0.27$ at $\kappa_2 = 300$. Notably, I for a $\kappa_2 = 300$ exceeds the maximum achievable I for a single-cavity system with $g = g_1$ (green dashed line), corresponding to the same V_{eff} . Though the improvement of ηI is less significant because of a reduced efficiency [Fig. 4(b)], ηI is still higher than what a single-cavity system allows.

We emphasize that, in both regimes, the timing dynamics are essential in understanding the improvement of I . The Purcell enhancement (LDOS) between the emitter and C_1 barely changes due to the presence of C_2 . The increase in I can be seen as a result of the modified time evolution of the Green's function that governs $\langle b^\dagger(t + \tau)b(t) \rangle$ [21].

Table I compares the η and I values achievable for the single- and cascaded-cavity architectures, assuming a silicon vacancy center in diamond at room temperature with $(\gamma, \gamma^*, \omega) \sim 2\pi$ (160 MHz, 400 GHz, 400 THz) [19], as a quantum emitter. To achieve I of ~ 0.95 in reg. 1, the single-cavity approach requires a very high Q factor of 50 000 000, which is technologically challenging, especially considering integration with the emitter. The cascaded-cavity system requires only $Q_1 = 7000$ for the first cavity and $Q_2 = 500000$ for the second cavity to achieve the same I . Reaching $I \sim 0.8$ requires only $Q_1 = 3600$ and $Q_2 = 50000$ for the cascaded-cavity system, whereas $Q = 10000000$ is needed for the single-cavity system. Note that, in both cases, the cascaded-cavity system also achieves much higher η values than the single-cavity case. In reg. 2, the highest ηI is found under the constraint of $Q_{\text{max}} = 500000$; the cascaded-cavity system then achieves an improved $\eta I = 0.311$ ($I = 0.315$) compared to the best single-cavity system ($\eta I = 0.266$, $I = 0.267$).

Finally, we statistically incorporate inhomogeneous broadening (spectral diffusion). Figures 5(a) and 5(b) plot I and η for reg. 1 and reg. 2 for different $\Delta\delta$ with fixed $\gamma^* = 10^4$. We used a Gaussian probability distribution to

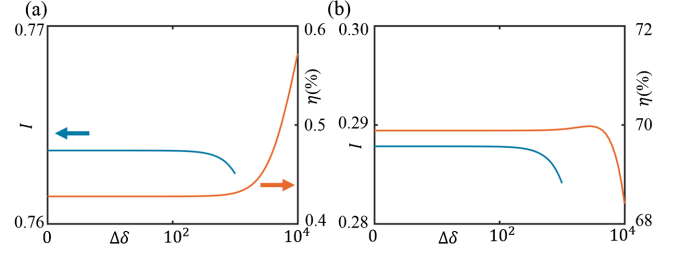


FIG. 5. I (blue line) and η (orange line) in the presence of spectral diffusion. (a) Reg. 1 ($g_1, \kappa_1, g_2, \kappa_2$) = (500, 50, 3, 10). (b) Reg. 2 ($g_1, \kappa_1, g_2, \kappa_2$) = (500, 50, 150, 300). In both regimes, spectral diffusion marginally affects the η and I . Note that the y axes in the figures are highly magnified to see the small change across the spectral diffusion.

model δ . The key observation here is that $\Delta\delta$ does not strongly diminish η and I when $\Delta\delta \ll \gamma^*$ (note that the vertical axis is highly magnified to show detail). This insensitivity to spectral diffusion follows from Eq. (1), which shows that the transfer rate (R_1) is reduced only by $\sim 2(\delta/\gamma^*)^2$ and, subsequently from Eq. (2), that the R_2 changed by a small amount. Suppression of the effect of small spectral diffusion happens only when the emitter is highly dissipative, i.e., if $\gamma + \gamma^* > \kappa$, and is a unique feature of the “cavity funneling” process. In other words, pure dephasing serves as a resource to stabilize the single-photon source, maintaining potentially high I and η despite spectral diffusion. This result is in contrast to the bare-emitter case, where the spectral diffusion directly affects I [18].

We emphasize the difference of our approach with the “photonic molecule” studied in Refs. [45,46]. In our cascaded-cavity system, the emitter couples only with the mode of C_1 , and the population is transferred between two cavity modes by weak coupling. In contrast, for the emitter coupled with a photonic molecule, the emitter is coupled to two supermodes that result from the strong coupling between two cavities, i.e., a splitting greater than the individual cavities’ decay rates. The cascaded-cavity system is also different than the hybrid-cavity system [36], where the cavity mode is modified by another cavity. More specifically, in a hybrid cavity, the latter cavity field acts as a electromagnetic environment (radiation bath) of the former cavity rather than as an independent cavity mode.

In conclusion, our analysis of funneling through a cascaded cavity revealed that it is possible to dramatically reduce the Q -factor requirements to the range of present-day feasibility. We derived closed-form analytical solutions that reproduce our numerical models. By incorporating pure dephasing and spectral diffusion, our analysis provides new insights into the modification of spontaneous emission in the bad-emitter limit of cavity QED. We also found that the cascaded-cavity approach greatly improves the quality of single photons emitted from quantum emitters, promising near-unity indistinguishability even

at room temperature that would be important in numerous applications such as photon-mediated entanglement [47,48]. Applied to low-temperature emitters, we expect that it should become possible to reduce photon distinguishability to reach near-unity fidelity in photon-mediated entanglement (see Supplemental Material [21]), which is essential for scalable quantum networks and proposed modular quantum computing architectures [49,50].

We thank Thomas Grange, Kevin A. Fischer, and Karl Berggren for helpful discussion. H. C. was supported in part by a Samsung scholarship and the Air Force Office of Scientific Research (AFOSR) Multidisciplinary University Research Initiative (MURI) on Optimal Quantum Measurements and State Verification. D. Z. was supported by the National Science Scholarship from Agency for Science, Technology and Research (A*STAR), Singapore. Y. Y. was supported in part by Skoltech as part of the Skoltech MIT Next Generation Program. D. E. acknowledges partial support from the Army Research Laboratory Center for Distributed Quantum Information (CDQI) and the Air Force Office of Scientific Research program (AFOSR) FA9550-16-1-0391, supervised by Gernot Pomrenke.

*choihr@mit.edu

†englund@mit.edu

- [1] I. Aharonovich, D. Englund, and M. Toth, *Nat. Photonics* **10**, 631 (2016).
- [2] P. Kok, W. J. Munro, K. Nemoto, T. C. Ralph, J. P. Dowling, and G. J. Milburn, *Rev. Mod. Phys.* **79**, 135 (2007).
- [3] M. Gimeno-Segovia, P. Shadbolt, D. E. Browne, and T. Rudolph, *Phys. Rev. Lett.* **115**, 020502 (2015).
- [4] M. Pant, D. Towsley, D. Englund, and S. Guha, *arXiv:1701.03775*.
- [5] V. Giovannetti, S. Lloyd, and L. Maccone, *Nat. Photonics* **5**, 222 (2011).
- [6] A. Aspuru-Guzik and P. Walther, *Nat. Phys.* **8**, 285 (2012).
- [7] S. Aaronson and A. Arkhipov, in *Proceedings of the Forty-Third Annual ACM Symposium on Theory of Computing* (ACM, San Jose, California, USA, 2011), pp. 333–342.
- [8] J. B. Spring, B. J. Metcalf, P. C. Humphreys, W. S. Kolthammer, X.-M. Jin, M. Barbieri, A. Datta, N. Thomas-Peter, N. K. Langford, D. Kundys *et al.*, *Science*, **339** 798 (2013).
- [9] K. Azuma, K. Tamaki, and H.-K. Lo, *Nat. Commun.* **6**, 6787 (2015).
- [10] M. Pant, H. Krovi, D. Englund, and S. Guha, *Phys. Rev. A* **95**, 012304 (2017).
- [11] P. Senellart, G. Solomon, and A. White, *Nat. Nanotechnol.* **12**, 1026 (2017).
- [12] Y.-M. He, Y. He, Y.-J. Wei, D. Wu, M. Atatüre, C. Schneider, S. Höfling, M. Kamp, C.-Y. Lu, and J.-W. Pan, *Nat. Nanotechnol.* **8**, 213 (2013).
- [13] N. Somaschi, V. Giesz, L. De Santis, J. Loredó, M. P. Almeida, G. Hornecker, S. L. Portalupi, T. Grange, C. Antón, J. Demory *et al.*, *Nat. Photonics* **10**, 340 (2016).
- [14] K. Müller, K. A. Fischer, C. Dory, T. Sarmiento, K. G. Lagoudakis, A. Rundquist, Y. A. Kelaita, and J. Vučković, *Optica* **3**, 931 (2016).
- [15] V. Giesz, S. L. Portalupi, T. Grange, C. Antón, L. De Santis, J. Demory, N. Somaschi, I. Sagnes, A. Lemaitre, L. Lanco *et al.*, *Phys. Rev. B* **92**, 161302(R) (2015).
- [16] H. Choi, M. Heuck, and D. Englund, *Phys. Rev. Lett.* **118**, 223605 (2017).
- [17] S. Hu and S. M. Weiss, *ACS Photonics* **3**, 1647 (2016).
- [18] F. W. Sun and C. W. Wong, *Phys. Rev. A* **79**, 013824 (2009).
- [19] E. Neu, C. Hepp, M. Hauschild, S. Gsell, M. Fischer, H. Sternschulte, D. Steinmüller-Nethl, M. Schreck, and C. Becher, *New J. Phys.* **15**, 043005 (2013).
- [20] J. Iles-Smith, D. P. McCutcheon, A. Nazir, and J. Mørk, *Nat. Photonics* **11**, 521 (2017).
- [21] See Supplemental Material at <http://link.aps.org/supplemental/10.1103/PhysRevLett.122.183602> for the master equation and optical Bloch equation of the system, adiabatic elimination and the rate equation, comparison of simulation results of the master equation and rate equation, derivation of the efficiency, effective emitter method, indistinguishability of regime 1, an exemplary diamond nanocavity design, effects of small g_1 , and a cascaded-cavity system with small dissipation and a large mode volume, which includes Refs. [22–33].
- [22] P. Knight and L. Allen, *Phys. Rev. A* **7**, 368 (1973).
- [23] H. Haug and A.-P. Jauho, *Quantum Kinetics in Transport and Optics of Semiconductors* (Springer, New York, 2008), Vol. 2.
- [24] A. Kiraz, M. Atatüre, and A. Imamoglu, *Phys. Rev. A* **69**, 032305 (2004).
- [25] S. Mouradian, N. H. Wan, T. Schröder, and D. Englund, *Appl. Phys. Lett.* **111**, 021103 (2017).
- [26] T. Iwasaki, F. Ishibashi, Y. Miyamoto, Y. Doi, S. Kobayashi, T. Miyazaki, K. Tahara, K. D. Jahnke, L. J. Rogers, B. Naydenov *et al.*, *Sci. Rep.* **5**, 12882 (2015).
- [27] T. Iwasaki, Y. Miyamoto, T. Taniguchi, P. Siyushev, M. H. Metsch, F. Jelezko, and M. Hatano, *Phys. Rev. Lett.* **119**, 253601 (2017).
- [28] S. Ditalia Tchernij, T. Luhmann, T. Herzig, J. Kupper, A. Damin, S. Santonocito, M. Signorile, P. Traina, E. Moreva, F. Celegato *et al.*, *ACS Photonics* **5**, 4864 (2018).
- [29] R. E. Evans, M. K. Bhaskar, D. D. Sukachev, C. T. Nguyen, A. Sipahigil, M. J. Burek, B. Machielse, G. H. Zhang, A. S. Zibrov, E. Bielejec *et al.*, *Science* **362**, 662 (2018).
- [30] A. M. Berhane, K.-Y. Jeong, Z. Bodrog, S. Fiedler, T. Schröder, N. V. Triviño, T. Palacios, A. Gali, M. Toth, D. Englund *et al.*, *Adv. Mater.* **29**, 1605092 (2017).
- [31] V. A. Soltamov, A. A. Soltamova, P. G. Baranov, and I. I. Proskuryakov, *Phys. Rev. Lett.* **108**, 226402 (2012).
- [32] T. T. Tran, K. Bray, M. J. Ford, M. Toth, and I. Aharonovich, *Nat. Nanotechnol.* **11**, 37 (2016).
- [33] C. Chakraborty, L. Kinnischtzke, K. M. Goodfellow, R. Beams, and A. N. Vamivakas, *Nat. Nanotechnol.* **10**, 507 (2015).
- [34] F. Peyskens, D. Chang, and D. Englund, *Phys. Rev. B* **96**, 235151 (2017).
- [35] S. Wein, N. Lauk, R. Ghobadi, and C. Simon, *Phys. Rev. B* **97**, 205418 (2018).

- [36] B. Gurlek, V. Sandoghdar, and D. Martín-Cano, *ACS Photonics* **5**, 456 (2018).
- [37] N.J. Turro, V. Ramamurthy, V. Ramamurthy, and J.C. Scaiano, *Principles of Molecular Photochemistry: An Introduction* (University Science Books, Sausalito, California, USA, 2009).
- [38] T. Grange, G. Hornecker, D. Hunger, J.-P. Poizat, J.-M. Gérard, P. Senellart, and A. Auffèves, *Phys. Rev. Lett.* **114**, 193601 (2015).
- [39] Y. Ota, S. Iwamoto, N. Kumagai, and Y. Arakawa, *Phys. Rev. Lett.* **107**, 233602 (2011).
- [40] S. Hu, M. Khater, R. Salas-Montiel, E. Kratschmer, S. Engelmann, W. Green, and S. Weiss, [arXiv:1707.04672](https://arxiv.org/abs/1707.04672).
- [41] A. Sipahigil, R. E. Evans, D. D. Sukachev, M. J. Burek, J. Borregaard, M. K. Bhaskar, C. T. Nguyen, J. L. Pacheco, H. A. Atikian, C. Meuwly *et al.*, *Science*, **354** 847 (2016).
- [42] J. L. Zhang, S. Sun, M. J. Burek, C. Dory, Y.-K. Tzeng, K. A. Fischer, Y. Kelaita, K. G. Lagoudakis, M. Radulaski, Z.-X. Shen *et al.*, *Nano Lett.* **18**, 1360 (2018).
- [43] A. Auffèves, D. Gerace, J.-M. Gérard, M. F. Santos, L. C. Andreani, and J.-P. Poizat, *Phys. Rev. B* **81**, 245419 (2010).
- [44] L. Fan, K. Y. Fong, M. Poot, and H. X. Tang, *Nat. Commun.* **6**, 5850 (2015).
- [45] A. Majumdar, A. Rundquist, M. Bajcsy, V.D. Dasika, S. R. Bank, and J. Vučković, *Phys. Rev. B* **86**, 195312 (2012).
- [46] A. Majumdar, A. Rundquist, M. Bajcsy, and J. Vučković, *Phys. Rev. B* **86**, 045315 (2012).
- [47] S. D. Barrett and P. Kok, *Phys. Rev. A* **71**, 060310(R) (2005).
- [48] P. C. Humphreys, N. Kalb, J. P. Morits, R. N. Schouten, R. F. Vermeulen, D. J. Twitchen, M. Markham, and R. Hanson, *Nature (London)* **558**, 268 (2018).
- [49] M. Pant, H. Choi, S. Guha, and D. Englund, [arXiv:1704.07292](https://arxiv.org/abs/1704.07292).
- [50] K. Nemoto, M. Trupke, S. J. Devitt, A. M. Stephens, B. Scharfenberger, K. Buczak, T. Nöbauer, M. S. Everitt, J. Schmiedmayer, and W. J. Munro, *Phys. Rev. X* **4**, 031022 (2014).